J Solid State Electrochem (2011) 15:455–472
DOI 10.1007/s10008-010-1124-7

REVIEW

The problem of Ru dissolution from Pt–Ru catalysts during fuel cell operation: analysis and solutions

Ermete Antolini

Received: 24 March 2010 / Revised: 31 May 2010 / Accepted: 9 June 2010 / Published online: 17 June 2010

Abstract Platinum–ruthenium catalysts are widely used as anode materials in polymer electrolyte fuel cells (PEMFCs) operating with reformate gas and in direct methanol fuel cells (DMFCs). Ruthenium dissolution from the Pt–Ru anode catalyst at potentials higher than 0.5 V vs. DHE, followed by migration and deposition to the Pt cathode can give rise to a decrease of the activity of both anode and cathode catalysts and to a worsening of cell performance. A major challenge for a suitable application of Pt–Ru catalysts in PEMFC and DMFC is to improve their stability against Ru dissolution. The purpose of this paper is to provide a better knowledge of the problem of Ru dissolution from Pt–Ru catalysts and its effect on fuel cell performance. The different ways to resolve this problem are discussed.

Keywords Pt–Ru catalysts · PEM fuel cells · Direct methanol fuel cells · Ruthenium dissolution · Durability

Introduction

Platinum–ruthenium (Pt–Ru) catalysts are generally regarded as the most appropriate materials for H_2/CO and CH_3OH electro-oxidation in acid environment [1–4]. For this reason, these catalysts have attracted considerable interest in recent years as anode materials for polymer electrolyte fuel cells (PEMFCs) operating with reformate gas [5–7] and for direct methanol fuel cells (DMFCs) [4, 8–10]. Because catalysis is a surface effect, the catalyst needs to have the highest possible surface area, so Pt–Ru catalysts are commonly used in the form of both unsupported and carbon supported (Pt–Ru/C) nanoparticles. It has to be promptly pointed out, however, that, while fully alloyed unsupported Pt–Ru nanoparticles are easily synthesized, supported Pt–Ru materials with a high degree of alloying are hardly obtained [11]. Indeed, binary Pt–Ru catalysts with Pt/Ru atomic ratio ≥1 can be prepared as fully alloyed (face centered cubic [*fcc*] PtRu alloys) [12], partially alloyed (*fcc* PtRu alloy and ruthenium oxide/hydroxide, RuO_xH_y) [11] and fully non-alloyed (*fcc* Pt and RuO_xH_y) [13] nanoparticles. The enhanced activity of Pt–Ru catalysts for carbon oxide and methanol oxidation, compared with that of Pt alone, has been attributed to both a bifunctional effect (promoted mechanism) [14, 15] and a ligand effect (electronic interaction between Pt and Ru, intrinsic mechanism) [9, 16]. According to the promoted mechanism, the oxidation of the strongly adsorbed oxygen-containing species is facilitated in the presence of Ru oxides by supplying oxygen atoms at an adjacent site at a lower potential than that accomplished by pure Pt. The intrinsic mechanism postulates that the presence of Ru modifies the electronic structure of Pt, and, as a consequence, the adsorption of oxygen-containing species or even the dissociative adsorption of methanol. For example, in the case of CO adsorption, an electron donation/back donation mechanism takes place. In the Pt–Ru alloys, a modification of the empty electron states density of Pt occurs, with a shift of the Fermi energy level with respect to the energy of CO molecular orbital. In such a situation, the synergic mechanism of interaction of Pt–CO bond looses its stabilizing effect. Ipo-electronic metals, like Ru, produce a

E. Antolini (✉)
Scuola di Scienza dei Materiali,
Via 25 aprile 22,
16016 Cogoleto, Genova, Italy
e-mail: ermantol@libero.it

E. Antolini
Instituto de Química de São Carlos, USP,
C.P. 780,
São Carlos, SP 13560-970, Brazil

shift effect and charge redistribution, which strongly influences the CO adsorption phenomena.

The optimum oxidation state of the Ru component in Pt–Ru catalysts for CO and CH_3OH oxidation is still a topic of discussion. While some authors refer to the active ruthenium compound mainly as metallic Ru^0 in PtRu alloys [11, 17, 18], different research revealed that the formation of a PtRu alloy is not an essential requirement for a high catalytic activity, and that hydrous ruthenium oxide is a more effective catalyst for the methanol oxidation reaction (MOR) than PtRu alloys [13, 19–21]. It remains an open question whether the bifunctional effect (operative in both Pt–RuO_xH_y and in PtRu alloys) or the electronic effect (present only in PtRu alloys) is predominant. As observed by Papageorgopolous et al. [22], the CO adsorbed on platinum sites needs to diffuse from platinum to ruthenium. In order for CO oxidation at Ru to take place at a considerable rate, platinum and ruthenium sites must be close enough together, but apparently not in the alloyed state. In recent years, Rolison et al. [13, 19, 23, 24] strongly advocated avoiding PtRu alloy; they found that the catalytic activity would increase by orders of magnitude if Ru existed in the hydrous oxides form in comparison with in alloyed form. The methanol oxidation reaction on Pt–RuO_xH_y catalysts occurs in the following way:

$$Pt + CH_3OH \rightarrow . \; Pt - (CO)_{ads} + 4H^+ + 4e^- \quad (1)$$

$$Pt - (CO)_{ads} + Ru - (OH)_{ads} \rightarrow Pt - Ru + CO_2 + H^+ + e^- \quad (2)$$

The benefits of RuO_xH_y were attributed to its electrons and protons conductibility and the innate possession of surface OH group. A study from Los Alamos National Laboratory [25] showed that the higher the RuO_xH_y content in Pt–Ru catalyst, the better the DMFC performance; in addition, Nafion was much less required in the anode because of the protonic conductivity of RuO_xH_y. However, they also pointed out that RuO_xH_y was not the prerequisite: indeed, high DMFC performance was also achieved in their work using completely alloyed Pt–Ru catalyst, in agreement with the work of Chu and Gilman [12].

The activity of Pt–Ru catalysts is a multivariate function of particle size, alloying degree, oxides composition, etc. The mono-dependencies of catalytic activity on individual structure parameters (structure-activity relationship (SAR)) are of great importance but unfortunately unobtainable in practical measurements. A pattern recognition methodology was proposed by Lu et al. [26] to extract SAR information from all relative experimental data. As a preliminary demonstration, multivariate linear regression and generalized regression neural network were applied to analyze a small dataset for methanol oxidation. As shown in Table 1 from ref. [26], it was found that both increasing the content of hydrous ruthenium oxides and decreasing particle size would benefit the catalytic activity, while the effect of PtRu alloy degree turned out to be unremarkable. Conversely, a negative effect of RuO_x on the methanol oxidation was found by Wu et al. [18]. They prepared electrochemically polarized Pt–Ru catalysts. The results indicated that the metallic state ($PtRu^0$)–Ru^0 can be formed during cathodic polarization and contributed to the MOR, while the formation of inactive ruthenium oxide during anodic polarization caused a negative effect on the MOR. These counteracting effects of ruthenium oxide on the MOR can be explained considering that the ruthenium oxides in Pt–Ru catalysts can be divided into two categories in terms of electrochemical reversibility, one reversible and the other irreversible. To evaluate the catalytic activity of reversible and irreversible RuO_xH_y, Lu et al. [27] carried out an anodic treatment of Pt–Ru/C catalysts in 0.5 M H_2SO_4 at 1.3 V vs. reversible hydrogen electrode (RHE) for 0.5 h. This treatment promoted the activity for methanol oxidation by a few tenths to five times. Based on the changes of cyclic voltammetry during the anodic treatment, a model was proposed for the activation effect. According to the model, there are two categories of ruthenium oxides, one is electrochemically reversible and beneficial for catalytic activity while the other is irreversible and harmful. During the anodic treatment, the harmful oxide is decreased while the beneficial oxide either increased or changed only slightly, resulting in a beneficial net change.

The durability of low-temperature fuel cells is a major barrier to the commercialization of these systems for stationary and transportation power applications. Commercial viability depends on improving the durability of the fuel cell components. Among them, electrode stability is a key factor limiting the commercialization of PEMFCs and DMFCs. PEMFCs typically use carbon supported nanome-

Table 1 The structure matrix and the activity matrix of different PtRu catalysts

Sample	Structure matrix			Activity matrix	
	m_{RuOxHy} (%)	1/ϕ (1/nm)	x_{Ru} (%)	0.4V	0.5V
1	2.56	0.25	10	32	185
2	2.18	0.23	45	9	63
3	0.90	0.28	30	5	41
4	0.51	0.26	47	9	65
5	3.89	0.36	27	51	295
6	3.55	0.48	38	61	329
7	2.36	0.37	3	22	133

Pt–Ru alloyed degree (Ru fraction in alloy, x_{Ru}), particle size (ϕ), and contents of hydrous Ru oxides (m_{RuOxHy}). Reproduced from Ref. [26], copyright 2005, with permission from the American Chemical Society

ter sized Pt and/or Pt alloy catalysts for both anode and cathode. Earlier studies [28, 29] showed that PEMFCs operating under constant potential for thousands of hours gradually lose catalytic active surface area by metal particle growth. For PEMFCs, a degradation range of 2–10 μVh^{-1} is common for most applications. Degradation rates of DMFCs are generally higher than that of PEMFCs, and depend on the application, but are typically in the range of 10–25 μVh^{-1}. Many works focused on the stability of Pt and Pt alloy cathode catalysts for oxygen reduction during fuel cell operation, and excellent reviews [30–33] deeply analyzed this issue. Compared with cathode catalysts, less works are addressed to the stability of Pt–Ru anode catalysts during fuel cell operation. While in PEMFCs it is well-known that cathode degradation, due to the higher potential and oxygen presence, is much more significant than anode degradation, in the case of DMFCs, where methanol is oxidized on the Pt–Ru catalyst surface, recent findings [34, 35] revealed that the two processes are linked. In the above-mentioned reports, it was found that the degradation of the anode can eventually result in the rapid deterioration of cathode performance, drastically reducing the overall efficiency of the fuel cell. In these Pt–Ru catalysts, significant Ru dissolution from the anode has been observed and the leached Ru ions were found not only in the polymer electrolyte membrane, but also deposited on the surface of the Pt cathode. As reported by Holstein and Rosenfeld [36], ruthenium loss from DMFC anodes can occur if the fuel cell is operated in a manner that results in ruthenium oxidation and reduction. For example, by increasing the anode potential to 1.0–1.2 V vs. RHE, anode potential lost during steady-state operation can be restored. High anode potentials might also occur when the fuel cell is turned off due to slow oxygen diffusion from the cathode under open circuit conditions. Return to normal operating conditions with high methanol flow returns the catalyst to the reduced state. Both deliberate cycling of the anode to high potentials and repeated cycling between on and off states could eventually lead to significant ruthenium loss from the anode and a slow degradation in DMFC performance. In the review of Petrii [8] on Pt–Ru catalysts only a very little part relates to Ru crossover during fuel cell operation. In the present work, an extended overview of the problem of Ru dissolution from Pt–Ru catalysts and its effect on fuel cell performance is presented. The different ways to resolve this problem are discussed.

Analytical methods to determine Ru dissolution from Pt–Ru catalysts following fuel cell operation

A broad array of instrumental techniques has been used to determine Ru dissolution from Pt–Ru catalysts. These analyses have been carried out on the Pt–Ru catalyst (to evaluate Ru loss), and on the membrane and the cathode (to evaluate Ru presence).

Ru loss from the Pt–Ru catalyst

The evaluation of Ru loss from the anode catalyst is complicate by the simultaneous dissolution of Ru and Pt atoms from the Pt–Ru catalyst. While in the case of Pt dissolution from the Pt catalyst the mass loss from the anode/cathode can be observed directly using an electrochemical quartz crystal microbalance, this technique cannot be used to evaluate Ru loss from Pt–Ru catalysts, because the simultaneous dissolution of Pt and Ru atoms from the catalyst. Spectrometric techniques, which determine the atomic composition of the catalysts, such as energy dispersive X-ray spectroscopy (EDX), inductively coupled plasma atomic emission spectrometry, atomic absorption spectrometry, and X-ray fluorescence spectrometry are often used to evaluate Ru dissolution, by comparison of the Pt/Ru atomic ratio before and after the stability test. As both Pt and Ru atoms dissolve from the Pt–Ru catalyst, this way to establish Ru dissolution is ambiguous: while the increase of the Pt/Ru atomic ratio clearly indicates Ru dissolution, Ru loss can occur also if the Pt/Ru atomic ratio is unchanged or decreased [37], depending on the relative amount of Pt and Ru lost. Comparison of X-ray diffraction (XRD) spectra of Pt–Ru before and after the durability test only shows the change in the amount of Ru alloyed. Indeed, Ru oxides generally are not detected by XRD. The increase of the lattice parameter is indicative of Ru dissolution from the PtRu alloy, but Ru loss can give rise to no increase of the lattice parameter if Pt and Ru atoms dissolve from the alloy in the same atomic ratio of the alloy. In this case, the lattice parameter is unchanged. Guo et al. [38] observed that the Ru alloyed increases following cell operation, also in the presence of Ru dissolution from the catalyst, meaning that part of non-alloyed Ru is lost and part alloyed with Pt.

Ru presence in the membrane and in the cathode

To evaluate Ru dissolution, analyses carried out on the membrane and on the cathode are more decisive than those on the anode. The presence of Ru atoms in the electrolyte and in the cathode can be revealed using the same techniques for identifying the elemental composition of the specimen or particular atoms reported for the determination of Ru dissolution from the anode. In this case the presence of Ru in the membrane and/or in the cathode is definitely indicative of Ru dissolution and migration. Secondary ion mass spectroscopy (SIMS) is a useful technique for the surface chemistry dealing with the adsorptions and reactions of adsorbed species in the model

systems. The unique advantages such as great sensitivity, detection of molecular cluster ions, and shallow information depth (1–2 nm) are further extending the applicability of SIMS in the field of the fuel cells. The research group at Samsung Advanced Institute of Technology, Korea [37, 39] successfully used time-of-flight secondary ion mass spectroscopy (TOF-SIMS) to visualize the surface molecular distributions as well as in-depth distribution of crossed ruthenium within the cathode catalyst layer at a microscopic scale. These works has demonstrated the great potential of TOF-SIMS in combination with X-ray photoelectron spectroscopy (XPS) in application of the fuel cells. They carried out durability tests on single DMFCs operating at 50 °C. The performances of three membrane electrode assemblies (MEAs) were monitored at different conditions to drive different performance degradations. The first sample (M1) with 17% performance drop was obtained by operating at 0.4 V vs. dynamic hydrogen electrode (DHE) for 2 h on each day over 114 h. The second MEA (M2) and the third MEA (M3) were aged over 136 and 128 h at 0.25 and 0.35 V vs. DHE, respectively. The evidence of Ru crossover can be obtained using XPS. Figure 1 from ref. [39] shows the XPS spectra of Pt *4f* and C *1s* for the cathode surfaces obtained from pristine and aged MEAs. The Pt 4f spectra showed little change with the performance degradation, which indicates that the oxidation of Pt at the cathode surface is not related to the performance loss. The C *1s* spectra displayed two main peaks for pristine and M1 cathode surfaces. A strong peak around 290 eV is assigned to the carbon in CF2 from Nafion ionomers, which was introduced in preparation of the catalyst layer. A peak at about 284 eV is ascribed to the carbon in hydrocarbons. For more deteriorated M2 and M3, another peak appeared at about 281 eV. This low binding energy peak can be attributed to Ru $3d_{5/2}$, and the peak at 284 eV becomes broader because of the superposition of the Ru $3d_{3/2}$ peak with the C *1s* peak. It is certain that the Ru traveled from the anode through the polymer membrane to the cathode surface. The atomic concentration of Ru accumulated on the cathode surface of aged MEA samples was less than 0.4 at.% based on quantitative XPS analysis. They investigated the vertical distribution to the membrane of traveled ruthenium within the catalyst layer of the cathode by TOF-SIMS with a peel-off method. They peeled off the cathode layer with a tape and obtained the mass-resolved ion images of the newly exposed surfaces using TOF-SIMS. Although it is difficult to estimate the thickness of the detached layer by a peel-off, the interface between the cathode catalyst layer and the membrane could be observed after the third peel-off by SEM. They believed that this peel-off method combined with a TOF-SIMS imaging technique could provide roughly the composition distribution with vertical depth to membrane by repeating the peel-off. Figure 2 from ref. [39] shows red green blue color overlays of mass-resolved ion images using TOF-SIMS for pristine (a) and M3 (b) cathodes with peel-off numbers. The Pt, Ru, and Nafion® ionomer distributions are expressed in red, green, and blue, respectively. Areas where the two or three components are present simultaneously appear as the relevant mixed color. For pristine cathode, the violet color remained within a whole catalyst layer of the cathode even though blue areas (Nafion®) increased slightly and red areas (Pt) decreased slightly with increasing peel-off numbers, that is, closely approaching the membrane. For the cathode in the M3 sample, the red color (Pt) diminished suddenly only after the first peel-off, green areas (Ru) increased, and blue (Nafion®) became dominant getting closer to the membrane. Summarizing, the Ru crossover was revealed by the XPS spectra and mass-resolved images of TOF-SIMS. The Ru species was not uniformly distributed within the catalyst layer of the cathode but accumulated more at the interface between the cathode catalyst layer and the gas diffusion layer, indicating the electrodeposition of cationic Ru species at this interface.

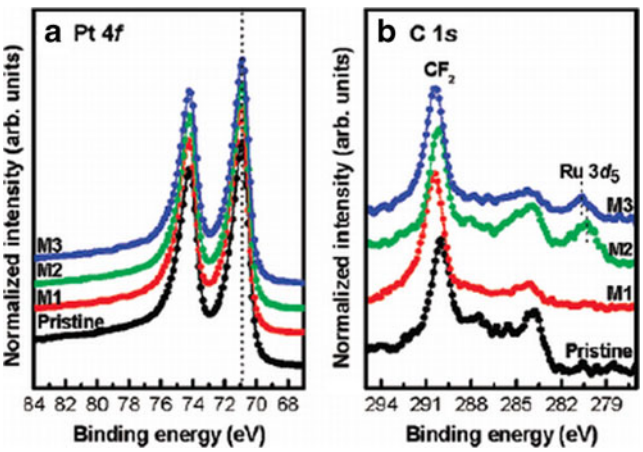

Fig. 1 **a** Pt *4f* and **b** C *1 s* XPS spectra for the surfaces of pristine and aged cathode catalyst layers. Reproduced from Ref. [39], copyright 2008, with permission from the American Chemical Society

Effects of Ru dissolution on the activity of fuel cell electrodes

Ru dissolution affects not only the performance of the anode, but also that of the cathode and the membrane. In the following parts of this section we analyze the effect of Ru dissolution on anode and cathode separately and on MEA.

Anode

In DMFCs, the anode potential for methanol electrooxidation on the Pt–Ru catalyst, at open circuit, is

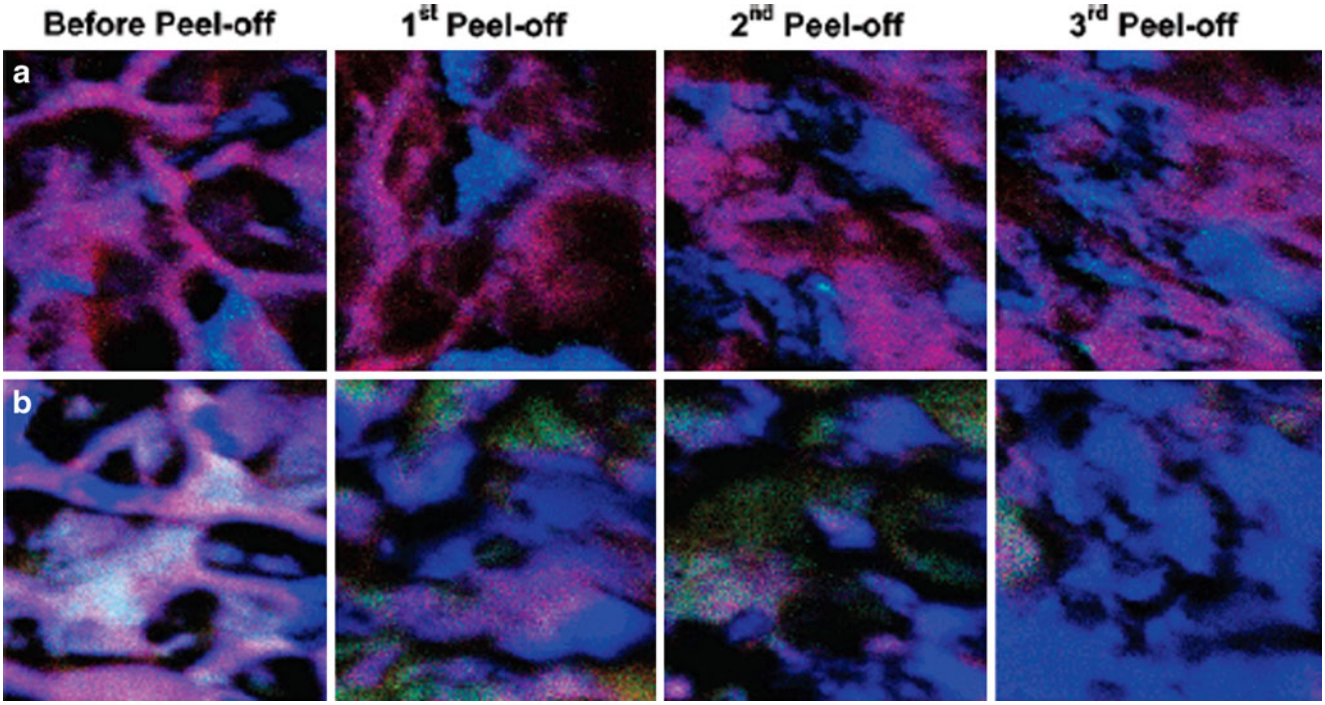

Fig. 2 RGB color overlay of the Pt (*red*), the Ru (*green*), and the Nafion (*blue*) for **a** pristine and **b** M3 cathodes with increasing peel-off times. Field of view: 500×500 μm^2. Reproduced from Ref. [39], copyright 2008, with permission from the American Chemical Society

approximately 0.2 V vs. DHE at 70–80 °C, and when the fuel cell operates under normal conditions, the anode potential value is in the range of 0.3–0.5 V vs. DHE [36]. Compared with the cathode potential, the anode potential normally has a relatively weak influence on the electrocatalysts. Thomas et al. [40] demonstrated an excellent stability of the anode at 100 °C (in addition to the anode stability already demonstrated at 80 °C) in DMFC. Unsupported Pt–Ru blacks of a nominal 1:1 Pt/Ru atomic ratio were used for anode preparation. Anode polarization data taken at the beginning and at the end of life test showed very small anode activity loss at 0.35 V vs. DHE. The observed drop in the rate of methanol oxidation at this potential over the 2,000-h life test was about 12%, from 0.285 to 0.250 A cm^{-2}. This change in the anode performance agrees well with a 12% change in the overall performance of the cell during the life test, thereby indicating that most performance loss incurred by the cell is due to a slow drop in the anode activity.

However, during long-term operation, short circuits, fuel starvation or cell reversal may occur, during which the anode may experience higher potentials higher than 0.5 V vs. DHE. Thus, different papers have been addressed to the effect of ruthenium loss from the Pt–Ru anode catalyst by repetitive potential cycling (RPC) up to 0.6–1.1 V vs. DHE on the activity for methanol and carbon monoxide oxidation [41–46]. Chen et al. [41] conducted a RPC on a partially alloyed Pt–Ru/C catalyst at 75 °C in potential regions of 0.2–0.5 V, 0.2–0.6 V, and 0.2–0.7 V vs. DHE, respectively (2,000 cycles for each region). The results showed that the RPC in the 0.2–0.5 V vs. DHE region, which simulates the anode potential under normal operating conditions, does not influence the Pt–Ru/C electrocatalyst, but when the upper limit of the potential region is elevated to 0.6 V or, in particular, 0.7 V vs. DHE, electrocatalyst degradation takes place. The remarkable degradation of the Pt–Ru/C electrocatalyst which occurred during the potential scan in the 0.2–0.7 V vs. DHE region was analyzed in detail. The results of the EDX analysis after an RPC in the 0.2–0.7 V vs. DHE region revealed an enhanced Pt/Ru weight ratio, indicating ruthenium dissolution from the electrocatalyst. The XRD analysis showed a negligible shift in peak positions of the PtRu alloy during the potential scan, indicating an insignificant Ru loss from the alloy. These results were explained on the basis of the dissolution of amorphous ruthenium hydrous oxide, which is not detected in the XRD patterns. RuO_xH_y is a mixed electron/proton conductor. Its loss leads to both an enhanced pure ohmic resistance and increased charge-transfer impedance for methanol oxidation, as revealed by the Nyquist diagram of anode electrochemical impedance spectrum (EIS). Figure 3 from ref. [41] shows the methanol-stripping curves before and after potential scan in 0.2–0.7 V vs. DHE region: with the cycle number increased, the methanol-stripping peak moved to the right, but the peak area reached its maximum value at the cycle number of 1,000 and then began to decline. The most probable reason for this phenomenon is that: at the

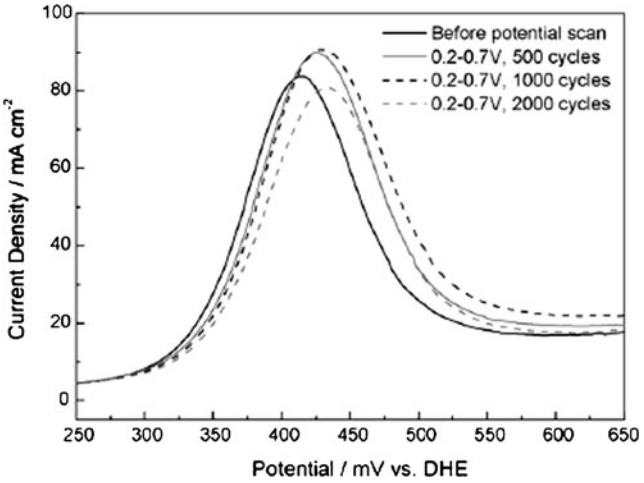

Fig. 3 Methanol-stripping curves before and after potential scan in 0.2–0.7 V vs. DHE region. Scan rate: 20 $mV s^{-1}$; temperature: 60 °C. Reproduced from Ref. [41], copyright 2006, with permission from Elsevier

beginning of the potential scan, the sudden dissolution of ruthenium left many small voids on the surface of the electrocatalyst, increasing the roughness of the catalyst surface, and, as a consequence its surface area. With the potential scan continuing, the small voids gradually vanished under the electrochemical stress. The variation in catalyst composition also influences the CO oxidation properties: after a potential scan in the 0.2–0.7 V region, the CO electro-oxidation peak became more Pt-like: in the first scan-cycle, when CO molecules were adsorbed onto the electrocatalyst, the hydrogen-desorption peak was almost completely suppressed. The CO electro-oxidation peak became narrower with a significant right-shift in the onset potential and maximum peak potential. These results strongly supports the assumption that ruthenium dissolved dramatically from the electrocatalyst during the potential scan in the 0.2–0.7 V vs. DHE region. Chakraborty et al. [42] prepared a flame synthesized mixed phase Pt–Ru catalyst. The flame synthesized Pt–Ru (1:1) consists of crystalline phases of metallic Pt or highly Pt rich PtRu alloys and Ru rich amorphous phases of Pt–RuO_x. To test the stability of this catalyst, the anode has been cycled between 0 and 0.8 V vs. DHE at 5 $mV s^{-1}$ for more than 30 h. Owing to Ru dissolution, the onset of methanol oxidation moved to ~45 mV more positive potentials compared with the relatively fresh anode. It can also be seen that below 0.55 V vs. DHE, the fresh anode performs better compared to the Ru depleted anode. However, for potential above 0.55 V, the Ru depleted anode shows much better performance. Shyam et al. [43] investigated the aging properties of two different commercial Pt–Ru black catalysts, Johnson-Matthey (JM) HiSpec6000 and Tanaka TEC90110, in 1 M trifluoromethanesulfonic acid with 0.3 M methanol as a function of both time and potential cycling. Following potential cycling between 0.02 and 0.8 V vs. RHE the Tanaka catalyst, which has relatively large RuO_xH_y islands on the surface, underwent little dissolution and agglomeration after 40 cycles. This had little detrimental effect on the CO oxidation properties, as seen by the CO stripping data. The JM catalyst, on the other hand, which has much smaller Ru islands, underwent more Ru dissolution/agglomeration, and showed definite signs of an increase in Ru island size and partial oxidation to RuO_xH_y. CO stripping curves for the two catalysts before and after an 8 h chronoamperometry session at 500 mV vs. RHE are shown in Fig. 4 from ref. [43]. In the case of the JM sample, there is a shift in the onset potential for the CO stripping, while there is no such shift for the Tanaka sample. Furthermore, a positive shift in the peak potential of ca. 50 mV is observed in both catalyst samples. It is clear that the two catalysts exhibit different aging characteristics, depending on their initial structure. Park et al. [44] compared the MOR activity of untreated and anodic-treated Pt–Ru catalysts with a Pt/Ru surface composition= 65:35, but with different content of RuO_xH_y. Before the cycles, the anodic-treated Pt–Ru electrodes and the untreated Pt–Ru electrodes have similar MOR activities. After 200 cycles (0.4–1.05 V vs. RHE at 500 $mV s^{-1}$), the untreated Pt–Ru electrodes showed a low Ru loss and a small decrease in the MOR activity. Conversely, the anodic-treated Pt–Ru electrodes showed both a high Ru dissolution and a remarkable decrease in methanol oxidation. Therefore, they ascribed the decrease of the MOR activity to the Ru dissolution from the Pt–Ru surface. Ma et al. [45] observed significant dissolution of RuO_xH_y species after RPC of Pt–RuO_xH_y(m)/MWCNTs (m being the Ru/Pt atomic ratio) catalysts in the potential region −0.20–

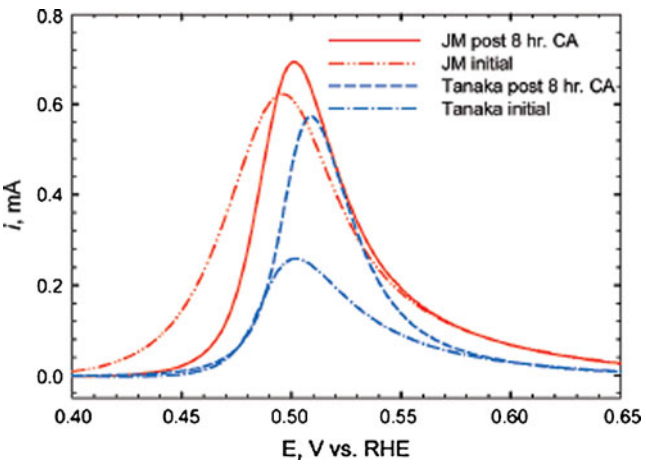

Fig. 4 CO stripping data 24 for the Johnson-Matthey (*red*) and Tanaka (*blue*) catalysts before and after an 8-h chronoamperometic test at 500 mV vs. RHE. The data have not been normalized for surface area. Reproduced from Ref. [43], copyright 2009, with permission from the American Chemical Society

0.96 V vs. SCE, resulting in reduced CO tolerance and a change in the activity order of $PtRuO_xH_y(m)$/MWCNTs catalysts for methanol electro-oxidation. In this case, Pt in the sample with $m = 0.20$, instead of that with $m = 0.1$, showed the highest catalytic activity. Sun et al. [46] investigated the effect of the changes in the composition and structure of Pt–Ru/C catalysts on the methanol electro-oxidation activity by RPC. With increasing the cycling number from 1 to 35, the peak potential of methanol oxidation gradually shifted to high potentials: this result was ascribed to the dissolution of Ru atoms from the surface of the Pt–Ru/C catalysts. With increasing the cycling number from 36 to 80, the Ru content of the catalysts was stable. However, the Pt–Ru particles size gradually increased, due to the moving and relocation of surface Pt atoms, resulting in a further decrease of the MOR activity.

Cathode

Piela et al. [34] provided electrochemical and X\RF evidence of ruthenium crossover in DMFCs using a state-of-the-art Pt–Ru catalyst at the anode. They found ruthenium susceptible to leaching out from the Pt–Ru black catalyst, crossing the proton-conducting Nafion® membrane and re-depositing at the Pt cathode on the opposite side of the fuel cell. After first detecting this phenomenon in a DMFC stack with a history of cell-voltage reversal, they since observed ruthenium crossover under virtually all DMFC operating conditions, from single cell break-in (humidification) to stack life testing. The degree of cathode contamination by Ru species depends on, among other factors, the DMFC anode potential and the cell operating time. To assess the impact of the Ru contamination on the cathode performance, firstly they carried out experiments, in which performance of a cell with a "Ru-free" cathode was evaluated in DMFC and H_2-air operating modes. Then, the cathode of the same cell was contaminated in the anode polarization mode, by holding the anode potential at 1.3 V vs. RHE for a prolonged time. Although entirely unrealistic from the fuel cell practice point of view (unless under cell-reversal conditions), that very high anode potential was used to merely accelerate the accumulation of ruthenium at the cathode surface, which would otherwise require operating a test cell for hundreds of hours. Following this "forced" contamination of the Pt cathode, H_2–air, and DMFC polarization plots were recorded and referred to the initial performance data in these two fuel cell operating modes. The results of such experiments are summarized in Fig. 5. The "forced" cathode contamination procedure did not affect the electrochemically active surface areas of either the cathode or the anode (cf. CO stripping data in Fig. 5a), nor did it impact the anode activity (cf. anode polarization plots in Fig. 5b). However, it did lead to a significant accumulation of the "Ru contaminant" at the cathode surface. In the H_2–air fuel cell operating mode, the cell voltage dropped by ~25 mV across the current density range used, which can be ascribed solely to lower cathode activity in oxygen reduction in the presence of the Ru contaminant at the surface (Fig. 5c). In the DMFC operating mode, the performance drop was more, ca. 40 mV (Fig. 5d). In addition to the loss in the activity for the oxygen reduction reaction (ORR), similar to that observed in the H_2–air operating mode, the additional ~15 mV voltage drop in the DMFC mode may indicate a loss in the cathode's ability to handle methanol crossover. Figures 5c and d also provide H_2–air and DMFC polarization plots recorded with a cell that had a cathode made from a Pt–Ru alloy catalyst rather than from a Pt black catalyst (open-square lines). These plots may be perceived as representing the maximum possible performance penalty caused by Ru crossover. In support of that statement, we stress here that the performance penalty caused by ruthenium crossover in the severely contaminated cell in the 22-cell DMFC stack was much more than either 25 or 40 mV. The cathode in that stack suffered a ca. 100 mV voltage loss in the kinetic region in DMFC operating mode: the performance of the reversed-cell cathode came close to the performance of a Pt–Ru alloy cathode. Gancs et al. [35] used rotating disk electrode (RDE) experiments to demonstrate the influence of dissolved Ru species on the oxygen reduction activity of a Pt/C electrocatalyst. Dissolved Ru in micromolar levels was found to deposit instantly onto Pt, thereby blocking the electrode surface for ORR at low overpotentials. Ru contamination can decrease oxygen reduction kinetics by eightfold or increase the overpotential by ca. 160 mV. Figure 6 from ref. [35] presents RDE polarization curves for the Pt/C thin-film electrode as recorded in oxygen-saturated 0–202 $\mu mol\,dm^{-3}$ Ru^{n+} electrolytes at the same scan direction and rate. Taking the measured current at 0.3 V as limiting current and plotting it as a function of the square root of the rotation rate, that is, by taking the Levich plot, a linear relationship could be obtained for all Ru concentrations. By looking at the half-wave potential values, which shift toward more negative electrode potentials in Ru^{n+}-contaminated electrolytes, as indicated by an arrow in Fig. 6, the changes become readily apparent on the reduction waves. The negative shift is maintained throughout the entire mixed-kinetics and mass-transport regime. The detrimental effect of Ru^{n+} contamination of the electrolyte on the ORR activity is evident even at the onset potential of ORR for clean Pt/C. Unlike the observed progressive decrease in surface oxide coverage on Pt with increasing Ru^{n+} contamination, oxygen reduction seems to occur on a minimum activity level beyond a certain Ru coverage on Pt. This is demonstrated in the overlapping

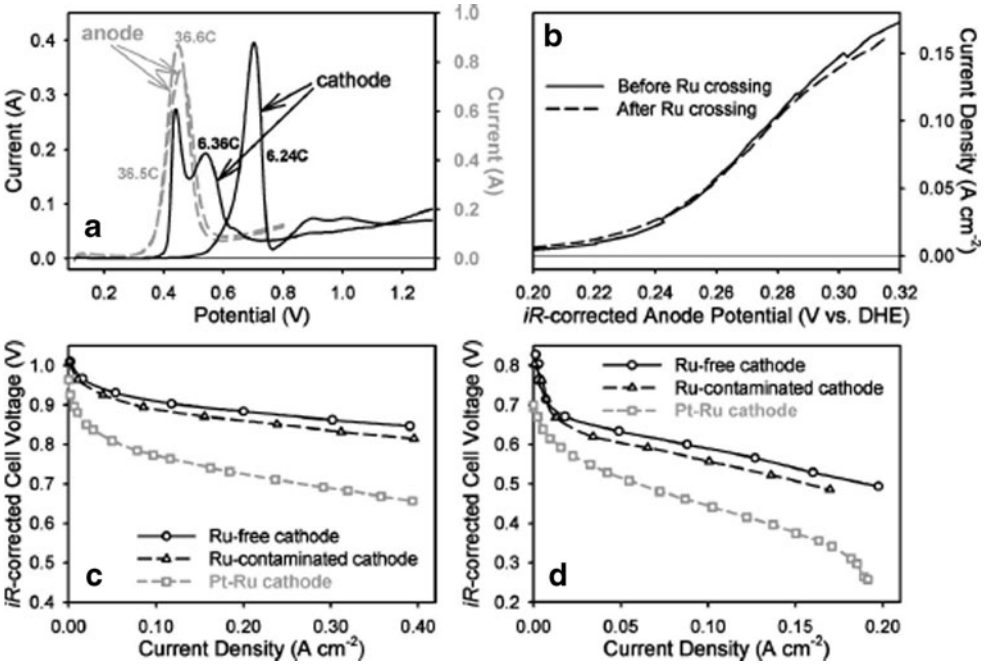

Fig. 5 Impact of ruthenium on oxygen reduction performance. **a** CO stripping scans for the cathode and anode, **b** steady-state anode polarization plots before and after contamination of the cathode, **c** H_2–air steady-state polarization curves, and **d** DMFC steady-state polarization curves. Methanol concentration 0.3 M, anode potential during contamination 1.3 V vs. hydrogen counter/*quasi*-reference electrode, cell temperature 75 °C. Reprinted from Ref. [34], copyright 2004, with permission from The Electrochemical Society

oxide reduction RDE curves for Ru^{n+} concentrations higher than 169 μmol dm^{-3} Ru^{n+}. Such a lower limit of ORR activity beyond a threshold Ru^{n+} concentration is attributed to the ability of Ru adatoms to reduce molecular oxygen at sufficiently high overpotential. Park et al. [47] investigated the impact of Ru on the cathode by adding Ru black externally to the Pt black cathode by 2 wt.%. The result of a single cell experiment by incorporating 2 wt.% Ru in the cathode was compared with that obtained with the pristine Pt black cathode. Conversely to the results previously reported, no appreciable variation in the decay rates with the incorporation of Ru in the cathode was observed.

Membrane electrode assembly

Low performance losses for MEAs with platinum electrodes in PEMFCs following duration tests have been reported. For example, Mukerjee and Srinivasan [29] observed a 2% performance loss after a duration test of 1,200 h at 200 mA cm^{-2}, and Wilson and Gottesfeld [48] less than 10% loss over almost 4,000 h at 0.5 V in maximum power density (MPD) of a PEMFC with low platinum loading catalyst layers. Among many factors that may be harmful to the stable operation of PEMFCs, the sintering of catalyst particles is one of the more important, decreasing the active area of the catalyst. The situation is even worse for DMFC, because in DMFC, the anode is fed with methanol solutions. The presence of liquids can accelerate the sintering process of catalyst particles, and methanol solution is aggressive to the Nafion® polymer electrolyte. So a long-term operation is more challenging for DMFC than for hydrogen gas-fed PEMFC [49]. In addition to the negative effect of methanol presence on the lifetime of the cell, Ru dissolution from the anode followed by Ru deposition on the cathode surface negatively affects the durability of a direct methanol fuel cell. In the last years, many works have been addressed to the global effect of Ru dissolution on the performance of the MEA in DMFCs [37, 38, 50–56]. Indeed, Ru dissolution simultaneously affects the performance of

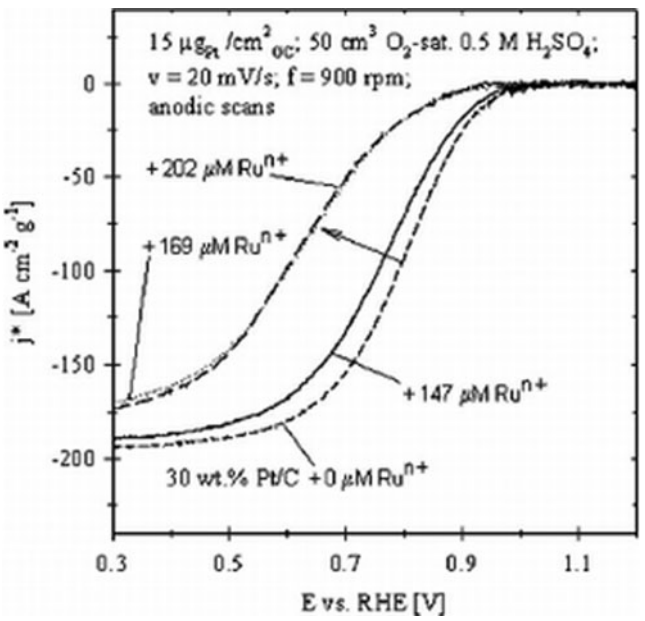

Fig. 6 Rotating disk electrode polarization curves for a thin-film 30 wt.% Pt/C electrode, 0.28 cm^2, 15 μg_{Pt} cm_{GC}^{-2} in O_2-saturated 0.5 mol dm^{-3} H_2SO_4 solution containing dissolved Ru species in various concentrations. Reprinted from Ref. [35], copyright 2007, with permission from The Electrochemical Society

anode and cathode and also of the membrane. Jeon et al. [50] carried out a stability test on DMFCs at different current densities for 145 h, using a Pt–Ru black catalyst with an original particle size of 3.3 nm for the anode electrode. The maximum power densities were 93.9%, 79.9%, and 55.1% of the initial value after operation at 100, 150, and 200 mA cm^{-2}, respectively. For the MEAs operated at 100, 150, and 200 mA cm^{-2}, the Pt–Ru particle sizes increased from the original size to 3.4, 3.9, and 4.2 nm, respectively, while a Pt black catalyst used for the cathode electrode did not change in size. Dissolution of the Ru was observed, and the Ru atomic fraction in the anode (x_{Ru}) changed from 0.47 in the case of the fresh MEA, to 0.46, 0.44, and 0.27 for the MEAs after operation at 100, 150, and 200 mA cm^{-2}, respectively. From the Ru atomic fraction before test (x_{Ruo}) and after duration tests at a current density j (x_{Ruj}), the amount of Ru loss (a_{Ruj}^{loss}) was calculated as:

$$a_{Ruj}^{loss} = 1 - x_{Ruj}(1 - x_{Ruo})/x_{Ruo}(1 - x_{Ruj}) \quad (3)$$

The effect of the amount of Ru loss on DMFC performance is shown in Fig. 7, obtained from data in ref. [49]. As can be seen in Fig. 7, a linear dependence of MPD loss on the logarithm of Ru loss was obtained.

The effect of durability tests on anode and cathode characteristics and DMFC performance are reported in Table 2. The performance loss widely ranged from 16% to 75% depending on test duration, potential and current density applied, and Pt–Ru structure.

Anode structural changes Generally, the EDX Ru/Pt atomic ratio decreases, due to RuO_xH_y loss and/or Ru dissolution from PtRu alloy [38, 50, 51, 53, 54]. Unusually, Park et al. [37] observed an increase of the EDX Ru/Pt atomic ratio, notwithstanding Ru loss from the anode: indeed Ru was found in the cathode. They explained this result supposing that Pt loss from the anode was higher than Ru loss. The XRD Ru/Pt atomic ratio, that is, the amount of Ru alloyed, also commonly decreases, due to dissolution of Pt and Ru atoms from the PtRu alloy, followed by redeposition of Pt atoms, but not of Ru atoms. Conversely, Guo et al. [38] found a decrease of the PtRu alloy lattice parameter, indicating an increase of the XRD Ru/Pt atomic ratio. Considering that the EDX Ru/Pt atomic ratio decreased, they supposed that part of non-alloyed Ru enters in the PtRu solid solution and partly dissolves from the anode catalyst. An increase of Pt–Ru particle size is commonly observed, and is ascribed to Ostwald ripening, being larger particles more energetically favored than smaller particles. Particle growth is supported by methanol presence. In some case, however, a decrease of Pt–Ru particle size was observed [37, 54]. According to Sarma et al. [54], the decrease in Pt–Ru grain size from fresh to the faded MEA may be attributed to the Ru loss from the catalyst during DMFC operation. Park et al. [37] by HR-TEM measurements observed that the Pt–Ru particles at the anode are decomposed into small particles through a morphological change (the Pt–Ru particles partly transformed from an initial spherical shape to a conical shape) and a cracking during the duration test.

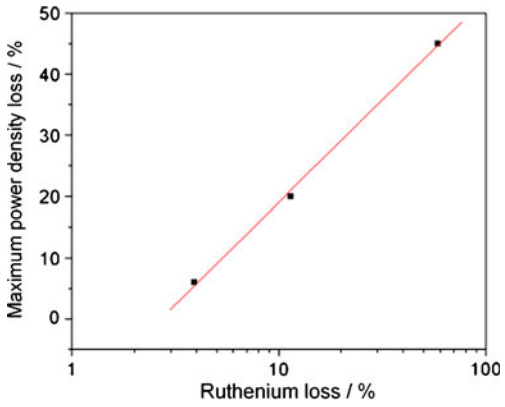

Fig. 7 Dependence of DMFC performance on Ru loss, obtained from data in ref. [49]

Cathode structural changes As to what happens to the Ru at the cathode, the electrochemical data suggest the occurrence of a slow deposition process of metallic Ru on Pt [34]. The surface acquires electrochemical properties that over time become Pt–Ru alloy-like. At submonolayer coverage levels, Ru is not expected to significantly impact the lattice parameters of the Pt crystallites. In XRD patterns, Pt cathode peak shift or generation of new peaks by formation of secondary phases were not observed [50, 55], that is, Ru does not form alloy with Pt or the amount of Ru in the alloy is very low. The question of how and in what form the crossover ruthenium is distributed within the cathode catalyst layer must remain open. According to Piela et al. [34], Ru is likely to fill the pores of the catalytic layer, some of it being in contact with the Pt particles. From the mass-resolved imaging technique of TOF-SIMS combined with a peel-off method, Chung et al. [39] found that ruthenium was not uniformly distributed within the cathode catalyst layer, but more accumulated at the surface of the catalyst layer, that is, the interface with the gas diffusion layer. XPS and TOF-SIMS results suggested that the ruthenium is electro-deposited as RuO*x* rather than metallic Ru. Conversely to the anode, Pt particle size always increases, and, as can be seen in Table 2, the cathode particle size more increased than anode particle size. The faster sintering rate of cathode catalyst is likely due to the higher potential at the cathode than at the anode. Another possible reason for the different growing rate of particles between anode and cathode is the different catalyst compositions. The anode catalyst is a bimetallic electro-

Table 2 Performance loss and change in electrode structure of DMFCs with Pt–Ru as anode catalyst and Pt as cathode catalyst following durability test

Anode/Stability test	Change in PtRu characteristics	Change in anode particle size/nm	Change in cathode particle size/nm	Performance loss/%	References
PtRu black (1:1)/128 h at 0.25 V vs. DHE, 50 °C	Increase of EDX Ru/Pt atomic ratio	Decrease 2.7–3.5→1.2–2.5	n.d.	45	[37]
45 wt.% PtRu/C (1:1)/2020 h at 100 mAcm^{-2}, 75 °C	Increase of Ru alloyed. Decrease of EDX Ru/Pt atomic ratio. RuO_xH_y, loss	Increase 1.8→2.8	Increase 3.3→6.3	75	[38]
PtRu black (1:1)/435 h at 150 mAcm^{-2}, 55 °C	Decrease of Ru alloyed. EDX Ru/Pt atomic ratio decrease	Increase 3.3→4.2	Increase 9.1→11.1	50	[51]
PtRu black (1:1)/160 h at 0.8 V vs. DHE, 40 °C	16.1% Ru loss (11.2% in Ru metal and 34.8% in RuO_2)	Slightly increase 2.4→2.7	Increase 2.4→4.2	26	[52]
45 wt% PtRu/CNT (1:1)/500 h at 70 mAcm^{-2}, 75 °C	Decrease of EDX Ru/Pt atomic ratio	Slightly increase 2.9→3.1	Increase 3.7→4.3	16	[53]
PtRu black (1:1)/600 h at 0.8 A, 40 °C	Decrease of EDX and XAS Ru/Pt atomic ratio	Decrease 2.1→1.7	Increase 6.5→8.1	n.d.	[54]
PtRu black (1:1)/110 h at 100 mAcm^{-2}, 60 °C	Decrease of Ru alloyed. Loss of Ru metal, RuO_2 stable	Increase 2.8→3.2	Increase 7.3→8.9	41	[55]
PtRu black (1:1)/2000 h at 100 mAcm^{-2}, 70 °C	Decrease of Ru alloyed	Increase 3.7→4.1	Increase 5.1→5.9	11 (MOR activity)	[56]
60 wt% PtRu/C (1:1)/2000 h at 100 mAcm^{-2}, 70 °C	Decrease of Ru alloyed	Increase 3.5→4.6	Increase 5.4→7.8	56 (MOR activity)	[56]

In all tests, Ru dissolution from Pt–Ru was detected

catalyst, in which ruthenium exists partly in the form of oxide or hydroxide, and these amorphous materials can inhibit the agglomeration of catalyst crystallites to some extent [53].

It was found that the electrochemical surface area (ECA) loss (determined by CV) is higher than the specific surface area (SSA) loss (determined by XRD) in both anode and cathode sides [53, 56]. Higher ECA loss might be caused due to the poisoning of catalysts by intermediates and impurities after durability test. The ECA loss estimates the real loss of cell performance while the SSA loss only represents the change of the microstructure such as agglomeration and growth of catalysts.

Ru presence within the membrane Lai et al. [52] showed by transmission electron microscopy (TEM) images Ru aggregation at the interface between the membrane and cathode catalyst. Figure 8 from ref. [52] reveals the bright-field TEM image for the particles (identified as Ru through EDX) distributed in the membrane near the cathode. The particle size was greater than that of Pt in the cathode catalysts (4.2 nm) and varied in the range of 10–100 nm. The particles distributed in the membrane near the cathode had a greater size than those distributed in the membrane far away from the cathode. Denser and greater particles of Ru distributed in the region near the cathode may be ascribed to vigorous reduction of Ru caused by a stronger electric field in this area compared to the regions far away from the cathode. Dense distribution of large-sized metallic Ru particles in the membrane possibly results in a plug on the paths for ionic

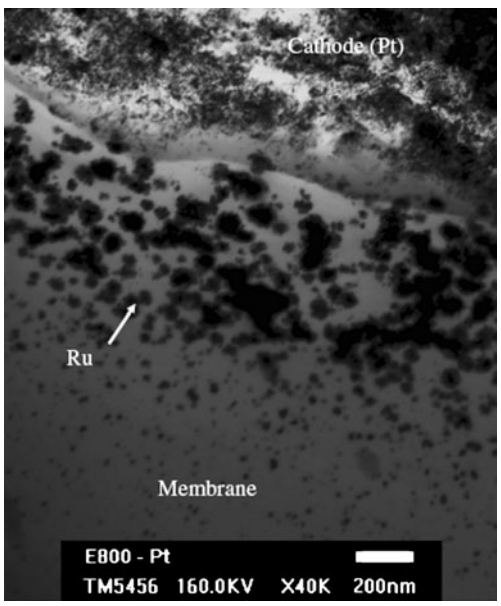

Fig. 8 Bright-field TEM image at the interface between the layer of cathode catalyst and the membrane after an accelerating degradation test at 0.8 V vs. DHE for 160 h. Reprinted from Ref. [52], copyright 2008, with permission from The Electrochemical Society

transportation (e.g., proton). This plug gives rise to an increase in the internal resistance of the system. The EIS results provided evidence to confirm this inference.

Effect of structural characteristics of Pt–Ru catalysts on Ru dissolution

As previously reported, Pt–Ru is stable at potentials up to 0.5 V vs. DHE (~0.8 V vs. RHE). Indeed, according to Pourbaix diagram for the Ru/water system [57], at 25 °C and assuming a pH for Nafion® between −0.3 and −0.2, metallic Ru is expected to be stable up to 0.8 V vs. RHE, with $Ru(OH)_3$ likely to form at even higher potentials. Hadzi-Jordanov et al. [58] investigated the stability of Ru surfaces (1) by cycling the electrode for various numbers of cycles from 0.05 V vs. RHE up to various anodic potentials (0.7, 0.9, 1.1, and 1.3 V vs. RHE) and (2) by establishing an anodic current in the range 6-16 mA. Appreciable anodic dissolution of Ru occurred on cycling over a potential range >0.7 V vs. RHE, especially to higher positive potentials. The dissolution was quite appreciable, especially during an anodic/cathodic cyclic treatment, when the anodic potential limit exceeds 0.8 V vs. RHE. This is the potential at which a higher state of surface oxidation begins to arise. Dissolution on steady-state anodic polarization was much less rapid. The effect of alloying of ruthenium with platinum, although small~free energy of the alloy formation ($-2\ kJmol^{-1}$) should lead to further stabilization of Ru in the electrode. No Ru dissolution from Pt–Ru electrodeposits in 0.5 M H_2SO_4 at room temperature was found by Gavrilov et al. [59] for anodic potential limits up to 1.1 V (RHE), in agreement with thermodynamic predictions. Indeed, ruthenium dissolution from thermodynamically stable Pt–Ru solid solution is even less probable than from pure Ru.

However, occasionally, the fuel cell may experience deep discharging processes or even a short circuit, and the anode potential value may reach 0.6 V or even as high as 0.7 V vs. DHE. High anode potentials might also occur when the fuel cell is turned off due to slow oxygen diffusion from the cathode under open circuit conditions. Another important phenomenon is the potential distribution at fuel cell anode. Recent double layer modeling of metal/solid polymer electrolyte interface demonstrates a possibility of dramatic potential fluctuations along the surface, with the amplitudes up to 0.3 V [60]. In all these cases, Ru dissolution from Pt–Ru catalysts can occur.

In Pt–Ru catalysts, Ru can be present in various forms, that is, as non-alloyed Ru metal, as Ru oxide/hydroxide, and alloyed with Pt to form PtRu solid solutions. The crystal structure of PtRu alloys is face centered cubic (*fcc*) up to Ru atomic fraction about 0.7, where Pt and Ru form a solid solution with Ru atoms replacing Pt atoms on the lattice points of the fcc structure. Above 0.7 at Ru, another solid solution is formed with Pt atoms replacing Ru in a hexagonal close packed (*hcp*) structure. Ruthenium dioxide, RuO_2, belongs to the family of transition-metal dioxide compounds with rutile structures. Pure RuO_2 is a metallic conductor due to a d-band conduction mechanism [61]. Single crystals of anhydrous RuO_2 exhibit conductivity on the order of $10^4\ Scm^{-1}$ at room temperature, due to an oxygen deficiency which is charge compensated by Ru^{3+} defects in the lattice. Unlike its anhydrous, crystalline parent rutile, hydrous ruthenium dioxide, RuO_xH_y, exhibits mixed electron–proton conductivity [62].

As reported in Section 3, Ru loss from the anode can occur by both RuO_xH_y loss and Ru dissolution from PtRu alloy. The following structural and chemical factors can affect the stability and support the dissolution rate of PtRu alloy and Ru oxidized forms: two-phase PtRu alloy composition (*fcc*+*hcp*), defectiveness and low stability of small particles and oxide non-stoichiometry. The relative stability of PtRu alloy and RuO_xH_y is an object of investigation. Generally, PtRu alloys are considered more stable than Ru oxides. Chang et al. [63] investigated the stability of RuO_xH_y by RPC in 0.1 M H_2SO_4 for 200 cycles, and the ratios of voltammetric charges between the *n*th and the first cycles (denoted as Q_n/Q_1) against the cycle number of CV are shown in Fig. 9 from ref. [63]. The scan rate of CV was $25\ mVs^{-1}$ and the potential window for this stability test was between 0 and 1.0 V vs. Ag/AgCl. The Q_n/Q_1 of the RuO_xH_y-coated electrode decayed very fast during the initial 40 cycles, and reached to 0.3 after the application of 200 cycles, revealing its instability. Ma et al. [45] prepared a series of Pt–RuO_xH_y catalysts containing 20% Pt using multi-walled carbon nanotubes (MWCNTs) as the support. The stability of these catalysts after RPCs in low (−0.20–0.46 V vs. SCE) and extended (−0.20–0.96 V vs. SCE) potential regions was investigated. In agreement with the results of Chang et al. [64], significant dissolution of RuO_xH_y species was detected after the RPC of Pt–RuO_xH_y/MWCNTs in the extended potential region. Park et al. [44]

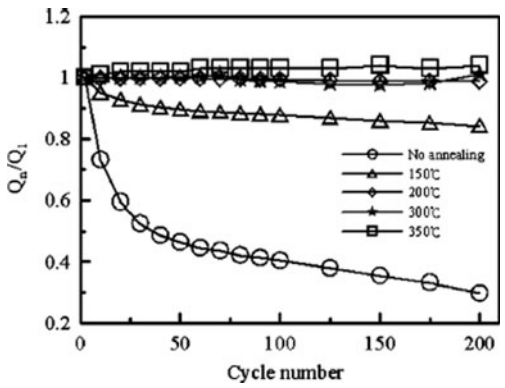

Fig. 9 The voltammetric charge ratios between the *n*th and the first cycle (Q_n/Q_1) against the cycle number of CV for pristine and annealed RuO_xH_y. Reprinted from Ref. [63], copyright 2004, with permission from The Electrochemical Society

studied the effect of ruthenium oxidation states on Ru dissolution from Pt–Ru thin-film electrodes by RPC (200 cycles) between 0.4 and 1.05 V vs. NHE). The Ru-oxidation states of the Pt–Ru thin films were systematically modified by an anodic (oxidation) treatment. The surface of Pt–Ru thin-film electrodes was altered and Ru-oxide species were formed. These oxide species were more easily dissolved than the alloyed Ru metal. By comparing the Ru $3p_{3/2}$ peak in the XPS spectrum for the anodic-treated Pt–Ru electrodes before and after RPC, they observed that the relative amounts of RuO_2 and hydrous RuO_2 decreased after the 200 cycles, implying that the Ru dissolution from the Pt–Ru electrode is caused by the Ru-oxide species. By comparing the aging properties of two different commercial Pt–Ru black catalysts, JM HiSpec6000 and Tanaka TEC90110, Shyam et al. [43] observed that the Tanaka catalyst, which presents relatively large RuO_xH_y islands on the surface, underwent little dissolution and agglomeration after 40 cycles. The Johnson-Matthey catalyst, on the other hand, which has much smaller Ru islands initially, underwent more Ru dissolution/agglomeration, and showed definite signs of an increase in Ru island size and partial oxidation to RuO_xH_y. It has to be remarked, however, that the higher stability of the Tanaka catalyst has to be ascribed overall to the larger islands.

Regarding the stability of PtRu alloys, an increase of the lattice parameter following different DMFC duration tests was observed [50, 54, 55], indicating Ru dissolution from the solid solution. A high degree of alloying, however, seems to be crucial for the achievement of Pt–Ru catalysts with low Ru loss during fuel cell operation. Gancs et al. [64] carried out a comparative elemental compositional as well as CO and CH_3OH electro-oxidation performance analysis on commercial Pt–Ru black catalysts having the same atomic ratio (1:1) but different degree of alloying. The results indicated that the latter physical property is crucial in maintaining the anodic activity for prolonged time. They concluded that a major factor leading to the chemical instability of Pt–Ru bimetallic electrocatalysts is due to the existence of hydrous RuO_2 and unalloyed Ru phases. Hyun et al. [65] prepared 60 wt.% Pt–Ru (1:1) catalysts with different degree of alloying. These catalysts were submitted to a RPC for 40 cycles. The Pt–Ru catalyst with the highest degree of alloying was the more stable. The shape of the CV curves of this catalyst during RPC less changed when compared with the other catalysts, implying a higher stability of the highly alloyed Pt–Ru catalyst with respect to the catalysts with a lower alloying degree.

Yamada et al. [66] investigated the effect of Ru content and phase alloy structure (fcc and hcp) on the stability of commercially available Pt–Ru/C catalysts of four different compositions (Pt/Ru atomic ratio=1:1, 2:3, 1:2, and 2:5, about 50 wt.%). The durability of these catalysts was examined by RPC between 0.05 V to 0.2 V vs. RHE in 0.5 M H_2SO_4 at 25 °C under argon atmosphere. The catalyst after the durability tests was analyzed by CV, and CO and Cu stripping voltammetry. While the voltammogram of the Pt–Ru (1:1)/C catalyst was stable even after 2,500,000 cycles, the peak area for hydrogen adsorption/desorption of other catalysts (Ru/Pt >1) gradually decreased. Cu and CO stripping voltammograms on Pt–Ru/C catalysts before and after potential cycling indicate that the Pt–Ru(1:1)/C has a high stability at potentials below 0.2 V vs. RHE in H_2SO_4. On the other hand, for the catalysts of Ru/Pt >1, the Cu and CO stripping peaks gradually decreased after potential cycling, and this tendency was enhanced with increasing Ru content. From these results it was inferred that part of Ru atoms on the surface were lost upon potential cycling when the Ru content exceeded the solubility limit of the Pt fcc phase. According to the authors, the observed instability of Pt–Ru/C (Ru/Pt >1) may be caused by the presence of the hcp phase or a difference in the degree of alloying or in the surface state (Ru oxide presence). In a succeeding work, Yamada et al. [67] carried out two kinds of durability tests in 0.5 M H_2SO_4 on Pt–Ru thin films with different Pt/Ru ratios (1:1 and 1:2) deposited on glassy carbon substrates. One is RPC between 0.05 to 0.2 V vs. RHE under hydrogen atmosphere. The other is constant potential holding tests in the range of 0.055 to 0.6 V vs. RHE for 12 days under argon atmosphere. XRD patterns of thin films with different Ru/Pt ratios showed that the Pt–Ru (1:2) thin film was a single phase of the hcp structure, while the Pt–Ru (1:1) thin films presented the fcc structure. During the potential cycling test, the Cu stripping peak at ca. 0.4 V vs. RHE, which originates from Cu_{upd} on Ru atoms, gradually decreased after 1,500,000 cycles and the Ru/Pt ratio of the outer-most surface, which was calculated from Cu stripping voltammetry peaks, decreased from 1.89 to ca. 0.89 after 4,500,000 cycles. Similar loss of surface Ru atoms were observed when the potential was kept at 0.2 and 0.55 V vs. RHE for 12 days, though the decrease in Ru/Pt ratio was less significant than that after RPC. For the fcc Pt–Ru (1:1) thin film, the decrease in surface Ru/Pt ratio was smaller than that for the hcp Pt–Ru (1:2). Regarding the influence of PtRu phase alloy on Ru dissolution, Gavrilov et al. [59] observed no Ru loss from Pt–Ru electrodeposits in 0.5 M H_2SO_4 at room temperature for anodic potential limits up to 1.1 V (RHE) for both single- (*fcc*) or two-phase (*fcc*+*hcp* at higher Ru content) alloy. Thus, they concluded that the type of phase alloy is hardly very important.

Solutions

Cathode contamination by Ru

Firstly, it is important to know if Ru contamination of the cathode is reversible. Piela et al. [34] investigated the effect

of cycling the potential between 0.1 and 1.3 V vs. RHE on the CO stripping peak position of a cathode slightly contaminated by Ru. After ten voltammetric scans at 5 $mV\,s^{-1}$, both the onset and peak potential of CO stripping shifted positively by ~35 mV, indicating partial removal of the Ru contaminant, possibly via anodic dissolution of ruthenium species at high cathode potentials. A similar effect was observed in a six-cell stack. The cathodes in this stack, initially slightly contaminated by ruthenium, showed an improvement following operation in the DMFC mode. A ca. 20 mV positive shift in the onset potential and peak potential of CO stripping from these cathode surfaces was detected in all cathodes in the stack. One possible path for Ru removal was related to the high potential of the air cathode for a prolonged cell operation time.

Apart its reversibility, Ru contamination at the cathode should be addressed either by novel anode catalysts with low Ru loss, by novel fuel cell designs such as the laminar-flow fuel cells [68, 69], where crossover is omitted, by less Ru-permeable membranes, or by more Ru-tolerant ORR electrocatalysts.

Ru dissolution from the anode

The key issue, however, is to resolve the problem of Ru dissolution from the Pt–Ru catalyst: Ru loss from the anode can be addressed either by highly stable Pt–Ru structures, by the use of suitable supports, or by the presence of stabilizing agents.

Highly stable Pt–Ru structures

Generally, *fcc* PtRu solid solutions are more stable than Ru oxi/hydroxide and/or *hcp* PtRu solid solutions [44, 64–67]. So, for stable long-terms fuel cell operation it is better to use fully fcc alloyed Pt–Ru catalysts, also if the performance could be slightly lower than that of non-alloyed Pt–Ru catalysts. Regarding RuO_xH_y, however, Chang et al. [63] found that its stability can be increased by suitable thermal treatments. They studied the effect of annealing on the stability of RuO_xH_y. The XPS spectra of Ru $3p_{3/2}$ and O *1 s* for RuO_xH_y untreated and annealed at 200 and 350 °C are shown in Fig. 10 from ref. [63]. The peaks of Ru $3p_{3/2}$ and O *1 s* shifted toward the lower binding energies when the annealing temperature increased. This shift in binding energies indicates that the amounts of RuO_2 and bridged oxygen (i.e., Ru–O–Ru) increase with the annealing temperature. The effect of annealing temperatures on RuO_xH_y can be estimated from the curve fitting of Ru $3p_{3/2}$ and O *1 s* spectra: anhydrous RuO_2 and hydrous RuO_2 increased and decreased, respectively, with increasing the annealing temperature. This result reveals the gradual transformation of hydrous oxide into the anhydrous when annealing is applied. The amount of RuO_3, instead, was

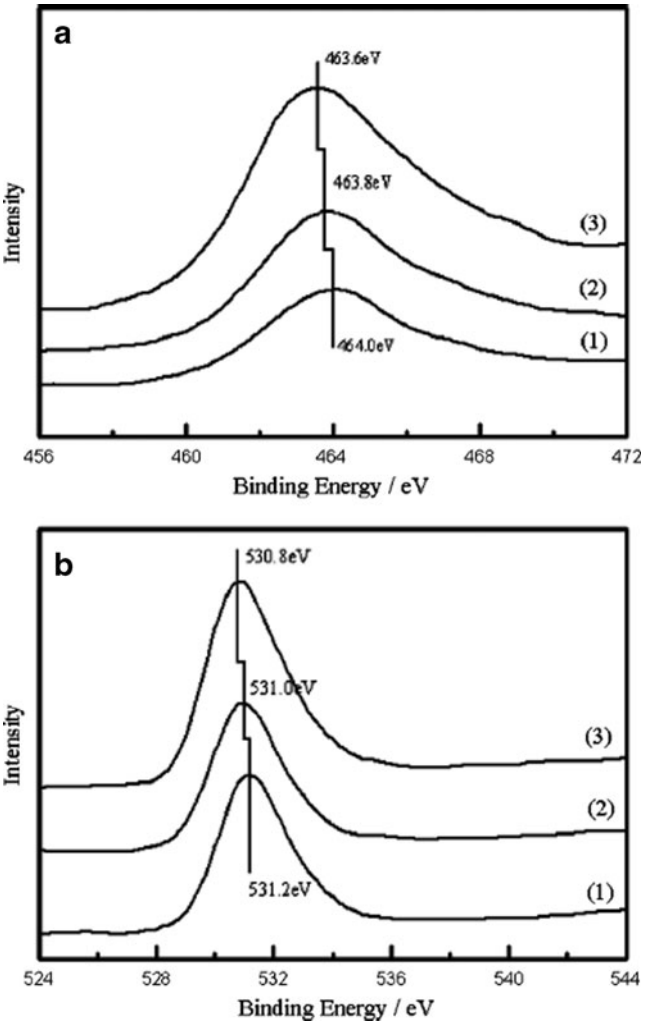

Fig. 10 XPS spectra of **a** Ru $3p_{3/2}$ and **b** O *1 s* for (*1*) pristine RuO_xH_y and RuO_xH_y annealed in air for 2 h at (*2*) 200 and (*3*) 350 °C. Reprinted from Ref. [63], copyright 2004, with permission from The Electrochemical Society

approximately independent of the thermal treatment, that is, RuO_3 was quite stable under the annealing conditions in this work. They proposed that RuO_3 species are trapped within the oxide matrix. Moreover, RuO_3 acted as an impurity in the oxide matrix, inhibiting the formation of RuO_2 crystals when RuO_xH_y was annealed in air at relatively high temperatures. As can be seen in Fig. 9 from ref. [63], Q_n/Q_1 of RuO_xH_y annealed at 150 °C reached 0.84 after the test of 200 CV cycles, and remained at least 0.95 for those annealed at temperatures ≥ 200 °C. Moreover, for RuO_xH_y annealed at temperatures ≥350 °C, a slight increase in Q_n/Q_1 was found. Thus, annealing does not only improve the electrochemical characteristics of RuO_xH_y but also enhances its stability, especially for those annealed at temperatures ≥200 °C.

Recently, high stability was showed by Pt–Ru catalysts formed by Pt metal and ruthenic acid or ruthenium oxide

nanosheets [70, 71]. Ruthenic acid nanosheet (HROns) electrodes have excellent electrochemical stability and are excellent proton-electron conductors. Due to the atomic level thickness of the nanosheets combined with the negative charge, the nanosheets can be considered as an inorganic macro anion [72]. Sugimoto et al. [70] reported the use of crystalline ruthenic acid nanosheets derived from $H_{0.2}RuO_{2.1}{\cdot}xH_2O$ as a co-catalyst for platinum towards CH_3OH and CO electro-oxidation in an acidic environment. The results indicated that the modification of Pt/C with HROns decreases the overpotential for CH_3OH electro-oxidation by ~150 mV and CO electro-oxidation by ~200 mV. A fourfold increase in methanol electro-oxidation activity was obtained from chronoamperometry at 500 mV vs. RHE. The increase in the activity was ascribed to the bifunctional characteristic of the surface of the HROns. This electrocatalyst is expected to provide superior durability compared to conventional Pt–Ru/C under fuel cell operating conditions due to the electrochemical stability of HROns. Saida et al. [71] prepared a ruthenium oxide nanosheets (RuO_2ns) modified Pt/C catalyst with composition of RuO_2/Pt = 0.5:1 (molar ratio). The stability of RuO_2ns-modified Pt/C and unmodified Pt/C were compared by an accelerated stability test (potential cycling between 0.05 and 1.2 V vs. RHE at 50 mVs^{-1} in 0.5 M H_2SO_4, 6 0 °C for 1,000 cycles). The ECA obtained from the hydrogen adsorption current for Pt/C decreased 75% after the stability test. In the case of RuO_2ns-Pt/C, the ECA decreased only 55% in comparison with initial state, showing that the presence of RuO_2ns increases the stability of Pt nanoparticles. After the accelerated potential cycling test, the methanol oxidation activity of Pt/C retained only ~14% of its initial activity, while, under the same stability test conditions, the methanol oxidation activity of RuO_2ns-Pt/C was ~70% of the initial mass activity. The results showed that the stability of Pt/C was dramatically increased by modification with RuO_2ns under the present experimental conditions. A tentative explanation on the role of RuO_2ns towards the enhanced stability is given on the basis of the strong acidic nature of RuO_2ns. RuO_2ns is intrinsically negatively charged ($[RuO_{2.1}]^{0.2-}$) and behaves as a solid acid, as indicated by the intercalation behavior of layered $H_{0.2}RuO_{2.1}$. Thus RuO_2ns should attract dissolved cationic Pt^{n+}, thereby acting as a protective layer inhibiting the diffusion of Pt^{n+} into the electrolyte.

Stabilized Pt–Ru catalysts by support effects

A comparison of the stability of carbon supported and unsupported Pt–Ru catalysts has been made by Cabello-Moreno et al. [73] and a significant benefit in stability of Pt–Ru/C catalysts was reported. Carbon supported Pt–Ru was more stable than the unsupported catalyst.

Wang et al. [74] deposited Pt–Ru electrocatalysts onto 1-aminopyrene (1-AP)-functionalized MWCNTs by a microwave-assisted polyol process. PtRu/1-AP-MWCNTs showed much better distribution with no formation of aggregates, higher electrochemically active surface area, and higher electrocatalytic activity for the MOR in DMFCs as compared to that on conventional acid-treated MWCNTs (AO-MWCNTs) and carbon black supported Pt–Ru electrocatalysts. Pt–Ru/1-AP-MWCNTs also showed significantly enhanced stability. The forward peak currents on Pt–Ru/1-AP-MWCNTs and Pt–Ru/AO-MWCNTs were measured as a function of the number of cycles performed from −0.2 to 1.0 V in 0.5 M H_2SO_4+1.0 M CH_3OH, and the results are shown in Fig. 11 from ref. [74]. In the case of Pt–Ru/1-AP-MWCNTs, the peak current remained almost constant from the 40th cycle to the 350th cycle after the initial increase. The peak current started to decrease gradually after the 350 cycles of potential scan. Using the current density measured after the 20th cycle as the reference, the anodic peak current of the 600th cycle was about 82% of that measured at the 20th cycle. The reduction in the electrocatalytic activity for methanol electro-oxidation on Pt–Ru/1-AP-MWCNTs was ~18%. In the case Pt–Ru/AO-MWCNTs, a poorer stability was observed. The peak current started to decrease quickly after about 50 cycles. The peak current of the 600th cycle was ~59% of the current density measured at the 20th cycle. The high anodic peak currents and much slower degradation in the anodic peak currents for the reaction on PtRu/1-AP-MWCNTs as compared to that on Pt–Ru/AO-MWCNTs demonstrated the significantly enhanced activity and stability of Pt–Ru electrocatalysts on 1-AP-MWCNTs. The increased stability also indicated that the attachment of Pt–Ru on MWCNTs via 1-AP as interlinkers is strong. The

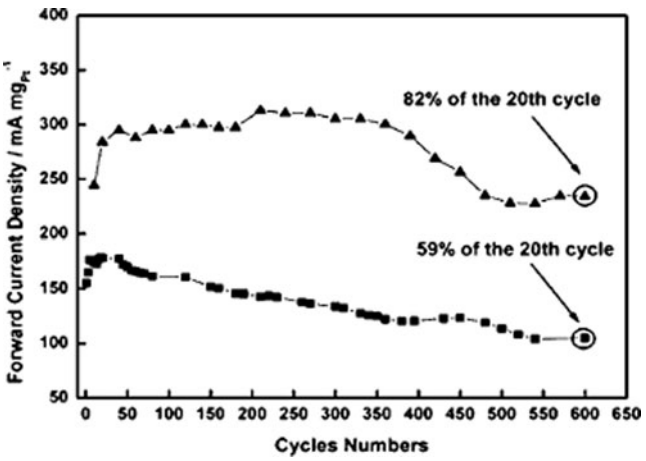

Fig. 11 Stability of Pt–Ru/1-AP-MWCNTs and Pt–Ru/AO-MWCNTs electrocatalysts in 0.5 M H_2SO_4 + 1.0 M CH_3OH. The potential scan was performed from −0.2 to 1.0 V vs. Ag/AgCl and the scan rate was 50 mVs^{-1}. (*filled triangles*) Pt–Ru/1-AP-MWCNTs, (*filled squares*) Pt–Ru/AO-MWCNTs. Reproduced from Ref. [74], copyright 2008, with permission from the American Chemical Society

results of this study demonstrated the promising potential of non-covalent functionalization of MWCNTs by 1-AP as highly efficient and effective catalyst supports. Liu et al. [75] synthesized Pt–Ru nanoparticles of ca. 2–3 nm on carbon mesoporous materials (Pt–Ru/CMMs) using SBA-15 mesoporous silica as the template, furfuryl alcohol and trimethylbenzene as the primary carbon source, and platinum and ruthenium acetylacetonates as the co-feeding metal and carbon precursors. XRD analysis indicated the formation of fcc PtRu alloys. The Pt–Ru(1:1)/CMM sample was found to possess the best electrocatalytic performance. The stability of the Pt–Ru(1:1)/CMM catalyst was evaluated by RPC (200 scan cycles of 3 min each) performed using 0.5 M H_2SO_4 with 1 M CH_3OH at room temperature. A nearly constant peak current density (measured at 0.60 V vs. Ag/AgCl) of the electro-oxidation of methanol accompanied by only a slight variation in I_f/I_r ratio was observed over the total scanned period of ca. 10 h, indicating a high stability of the Pt–Ru nanoparticles.

Stabilized Pt–Ru catalysts by the presence of an additive

It was found that the addition of oxides, such as SiO_2, TiO_x, and WO_x, to the Pt–Ru catalysts increase the long-term stability of both PtRu alloys [76, 77] and Pt–RuO_xH_y [78], preventing aggregation and/or agglomeration of the Pt–Ru partcles, and Ru dissolution from the catalytic surface. Shimazaki et al. [76] prepared a highly stable DMFC anode catalyst by adsorbing silica-immobilized Pt–Ru (1:1) nanoparticles on carbon support. The silica was immobilized on the Pt–Ru nanoparticles surface by a condensation reaction of sodium silicate. XRD analysis indicated PtRu alloy formation. STEM-EDX measurements proved existence of silica on the surface of Pt–Ru nanoparticles. The electrode with the silica-immobilized Pt–Ru nanoparticles presented a MOR activity comparable to that with a commercial catalyst. The electrochemical stability of the catalyst was estimated by measuring the methanol oxidation current after immersion of the working electrode in 1.5 M H_2SO_4 acid solution for a given time. As shown in Fig. 12 from ref. [76], the activity of Pt–Ru–SiO_2/C was maintained for 1,000 h, while the activity of the Pt–Ru/C catalyst decayed after 100 h, showing high durability of the silica-immobilized Pt–Ru nanoparticles in quasi-anodic acidic environment. Tian et al. [77] prepared a Pt–Ru–TiO_x/C electrocatalyst by a modified polyol synthesis method, followed by thermal treatment at 500 °C for 2 h under reductive atmosphere to enhance the interaction between the metal particles and the support. A 90-h lifetime test of the DMFC, carried out at the current density of 100 mA cm^{-2} and 75 °C, showed that Pt–Ru–TiO_x/C-500 has better durability than a commercial Pt–Ru/C, which may be attributed to the addition of titanium oxide, improving the

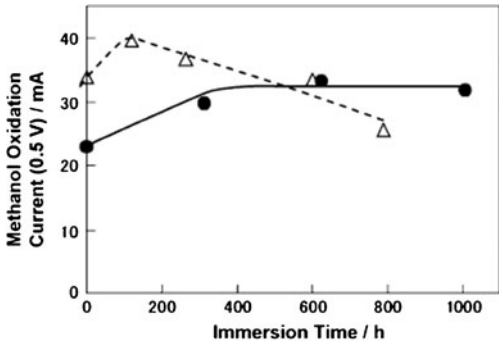

Fig. 12 Plots of methanol oxidation current against immersion time of electrodes to sulfuric acid solution; (*filled circles*) silica-immobilized PtRu nanoparticles catalyst, (*empty triangles*) silica-free citrate-stabilized PtRu nanoparticles catalyst. Reproduced from Ref. [76], copyright 2006, with permission from Elsevier

interaction between noble metal particles and the support. Ma et al. [78] found that the dissolution of RuO_xH_y in Pt-based catalyst during RPC in the potential range between −0.20 and 0.96 V vs. SCE can be reduced remarkably by addition of tungsten oxide (WO_x) to a MWCNT supported Pt–RuO_xH_y catalyst. Ruthenium dissolution was reduced from 70% in the reference Pt–RuO_xH_y/MWCNTs catalyst down to 15% in the Pt–RuO_xH_y–WO_x/MWCNTs. In this

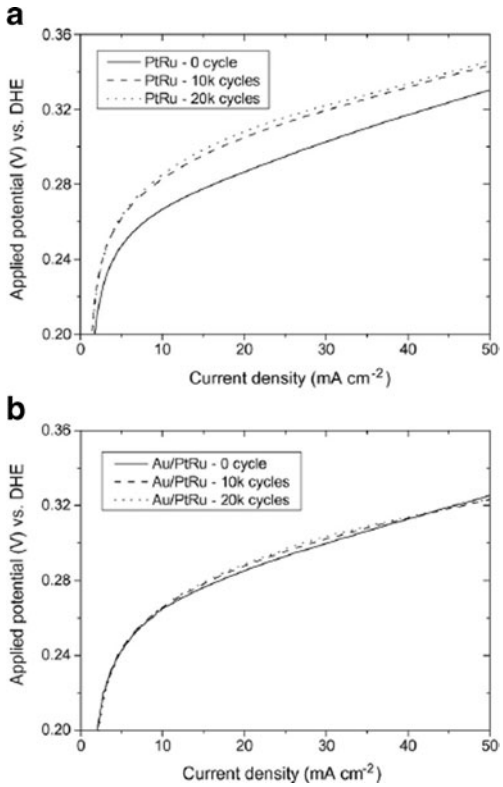

Fig. 13 The change of the anode polarization curves of the Pt–Ru catalyst and the Au/Pt–Ru catalyst during the course of potential cycling: **a** the Pt–Ru catalyst and **b** the Au/Pt–Ru catalyst. Reproduced from Ref. [81], copyright 2008, with permission from Elsevier

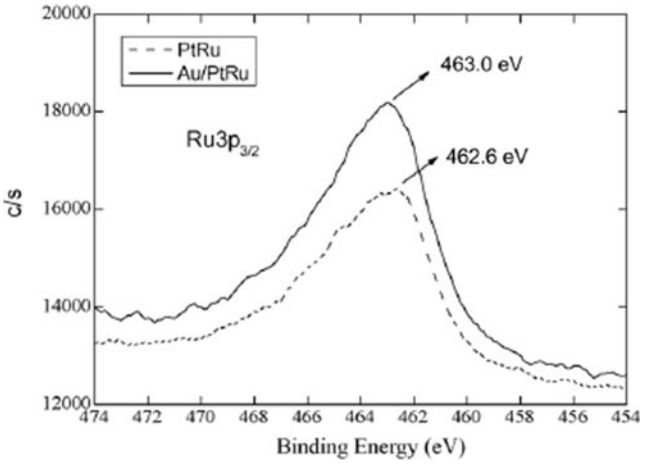

Fig. 14 XPS spectra of Ru $3p_{3/2}$ of the Pt–Ru catalyst and the Au/Pt–Ru catalyst. Reproduced from Ref. [81], copyright 2008, with permission from Elsevier

work, WO_x and RuO_xH_y in Pt–RuO_xH_y–WO_x/MWCNTs were generated simultaneously in the presence of H2O2. This makes it possible to provide abundant interfaces between WO_x and RuO_xH_y. The improved stability of RuO_xH_y in the acid electrolyte could be ascribed to its contact with adjacent WO_x.

Park et al. [79] reported the effect of $FePO_4$ coating on Ru dissolution from the Pt–Ru thin-film electrodes: unlikely from the previously reported oxides, $FePO_4$ does not prevent Ru dissolution from the Pt–Ru electrode, but prevents the diffusion of dissolved Ru species into the electrolyte. They investigated the effects of $FePO_4$ nano-scale coating on PtRu thin films on the block of Ru crossover. Ru dissolution was investigated by the accelerated potential cycles between 0.4 and 1.05 V vs. SCE at a scan rate of 500 $mV\,s^{-1}$ for 200 cycles. The results showed that Ru dissolution from $FePO_4$-coated Pt–Ru surface was inevitable due to the direct contact between the Pt–Ru surface and aqueous electrolyte. However, the $FePO_4$ coating layer on Pt–Ru thin-film electrodes effectively retained the dissolved Ru species, thus preventing the dissolved Ru species from diffusing into the electrolyte. Moreover, the retained Ru species within the $FePO_4$-coating layer were redeposited onto the Pt–Ru surface during the cycling in the fresh electrolyte. Ru redeposition, however, did not affect the methanol oxidation activities, probably by not forming the ideal PtRu solid solution.

Recently, Zhang et al. [80] found that the platinum nanoparticles could be stabilized against dissolution by depositing gold on the surface: the improved stability was achieved by the higher platinum oxidation potential resulted from the gold clusters. On this basis, Liang et al. [81] prepared an Au-modified Pt–Ru catalyst (Au/Pt–Ru) and found that the incorporation of Au significantly stabilizes the Pt–Ru electrocatalyst against Ru dissolution. The dissolution of Ru from the Pt–Ru and the Au/Pt–Ru catalysts was studied by RPC from 0.20 to 0.80 V vs. DHE at the scanning rate of 0.20 $V\,s^{-1}$. Figure 13 from ref. [81] shows the change of the anode polarization curves of the Pt–Ru catalyst and the Au/PtRu catalyst during the course of the potential cycling. From Fig. 13a, it can be seen that the anode overpotential of the Pt–Ru catalyst increased by 20 mV after 10,000 cycles of potential cycling. In contrast, however, the anode polarization curve of the Au/Pt–Ru catalyst showed negligible changes during the potential cycling test, as shown in Fig. 13b. The higher electrochemical stability of the Au/Pt–Ru catalyst was also observed by methanol stripping measurements. To know how the incorporation of Au into the Pt–Ru catalyst can stabilize the Pt–Ru catalyst, they compared the XPS spectra of Ru $3p_{3/2}$ of Pt–Ru and Au/Pt–Ru catalysts, as shown in Fig. 14 from ref. [81]. A positive shift of 0.4 eV in the binding energy of Ru $3p_{3/2}$ after the incorporation of Au indicated that the electronic structure of Ru was altered and a charge transfer flew from Ru to Au. As the electron loss in Ru increases the oxidation state of Ru, the oxidation of Ru ($Ru=Ru^{3+}+3e^{-}$) in the Au/Pt–Ru

Table 3 Factors improving the stability of Pt–Ru catalysts

Parameter	Type	Stability	References
Pt–Ru structure	Fcc PtRu alloys	Fcc PtRu alloy>Pt–RuO_xH_y	[44, 64–67]
	Annealed RuO_xH_y	Annealed RuO_xH_y>untreated RuO_xH_y	[63]
	HROns–Pt and RuO_2ns–Pt/C	High stability of HRO and RuO2 nanosheets. (RuO_2ns)–Pt/C>Pt/C	[71]
Support	Carbon	PtRu/C>PtRu	[73]
	1-AP-MWCNT	PtRu/AP-MWCNTs>PtRu/MWCNTs≈PtRu/C	[74]
	CMM	High stability	[75]
Additive	SiO_2	Pt–Ru–SiO_2/C>Pt–Ru/C	[76]
	TiO_x	Pt–Ru-TiO_x/C-500>Pt–Ru/C	[77]
	WO_x	Pt–RuO_xH_y–WO_x/MWCNT>Pt–RuO_xH_y/MWCNTs	[78]
	$FePO_4$	$FePO_4$ prevents the diffusion of dissolved Ru species into the electrolyte	[79]
	Au	Au/Pt–Ru>Pt–Ru	[81]

catalyst requires much higher potentials than in the unmodified one. As a result, the dissolution of Ru can be reduced by the incorporation of Au. Comparison of the Ru *3p* and Pt *4f* XPS reflexions of the cathode catalyst after RPC for 20,000 cycles indicated that considerable amount of Ru was present in the cathode catalyst assembled with Pt–Ru as the anode catalyst, whereas only traces of Ru existed in the cathode catalyst assembled with Au/Pt–Ru as the anode catalyst.

The different ways to improve the stability of Pt–Ru catalysts are summarized in Table 3.

Conclusions

Pt–Ru catalysts are substantially stable at the commonly used fuel cell anode potentials, lower than 0.5 V vs. DHE. But for different reasons, the potential can overcome 0.5 V vs. DHE. In this case, Pt–Ru is not stable and Ru dissolution can occur. Ru loss affects the catalytic activity of both anode and cathode catalysts. *Anode:* generally, the MOR activity of Pt–Ru catalysts decreases with Ru loss [41–46]. Indeed, the nominal Pt/Ru atomic ratio of the PtRu catalyst is in the optimum composition 1:1, so a decrease in Ru content in the catalyst results in a decrease of the MOR However, depending on the degree of alloying, the MOR activity of the Pt–Ru catalyst should also increase following Ru loss. *Cathode:* generally, the ORR activity of the cathode decreases owing to the presence of Ru [34, 35], but no effect of Ru contamination on the ORR activity of Pt was also observed [47]. Once deposited at the cathode, ruthenium inhibits oxygen reduction kinetics and the catalyst's ability to handle methanol crossover. Depending on the degree of cathode contamination, the overall effect of ruthenium crossover on cell performance may be from as little as ~40 mV up to 200 mV. *MEA:* the overall fuel cell performance always decreases, with a performance loss going from 16% to 75%, depending on the duration and/or applied potential/current of stability tests, on the MEA characteristics and/or on the Pt–Ru catalyst structure.

There is a generally consensus regarding the higher stability of alloyed ruthenium than that ruthenium oxi/hydroxide [44, 64–67]. For this reason, also if the catalytic activity of non-alloyed Pt–RuO_xH_y seems to be higher than that of alloyed PtRu, the use of PtRu alloys is recommended for higher fuel cell performance stability during long-term fuel cell operation. However, the stability of RuO_xH_y can be increased by thermal treatments at suitable temperatures [63].

The cathode contamination can be reduce both by reducing Ru dissolution from the anode, and, independently of Pt–Ru catalyst, by novel fuel cell designs such as the laminar-flow fuel cells [68, 69], where crossover is omitted, by less Ru-permeable membranes, or by more Ru-tolerant ORR electrocatalysts.

Different solutions have been proposed to address the problem of Ru dissolution from the Pt–Ru catalyst, including highly stable Pt–Ru structures [63, 70, 71], the use of suitable supports [74, 75], or the presence of stabilizing agents [76–79, 81]. The use of ruthenium oxide in nanosheet form [70, 71] and the addition of gold to the Pt–Ru catalyst [81] seem to be the most promising solutions. A powerful way to greatly reduce Ru dissolution from Pt–Ru catalysts could be to join different stabilizing factor, that is, a stable Pt–Ru structure with a suitable support and a stabilizing agent.

Acknowledgments The author thanks the Conselho Nacional de Desenvolvimento Científico e Tecnológico (CNPq, Proc. 310151/2008-2) for financial assistance to the project.

References

1. Gasteiger A, Markovic N, Ross PN, Cairns EJ (1994) J Phys Chem 98:617
2. Ianniello R, Schmidt VN, Stimming U, Stumper J, Wallau A (1994) Electrochim Acta 39:1863
3. Iwasita T (2002) Electrochim Acta 47:3663
4. Wasmus S, Kuver A (1999) J Electroanal Chem 461:14
5. Oetjen HF, Schmidt VF, Stimming U, Trila F (1996) J Electrochem Soc 143:3838
6. Antolini E, Giorgi L, Cardellini F, Passalacqua E (2001) J Solid State Electrochem 5:131
7. Antolini E (2004) J Appl Electrochem 34:563
8. Petrii OA (2008) J Solid State Electrochem 12:609
9. Arico AS, Srinivasan S, Antonucci V (2001) Fuel Cells 1:133
10. Liu H, Song C, Zhang L, Zhang J, Wang H, Wilkinson DP (2006) J Power Sources 155:95
11. Antolini E (2003) Mater Chem Phys 78:563
12. Chu D, Gilman S (1996) J Electrochem Soc 143:1685
13. Long JW, Stroud RM, Swider-Lyons KE, Rolison R (2000) J Phys Chem B 104:9772
14. Markovic NM, Gasteiger HA, Ross PN, Jiang X, Villegas I, Weaver MJ (1995) Electrochim Acta 40:91
15. Goikovic SL, Vidakovic TR, Durovic DR (2003) Electrochim Acta 48:3607
16. Christensen PA, Hamnett A, Troughton GL (1993) J Electroanal Chem 362:207
17. Hamnett A (1997) Catal Today 38:445
18. Wu G, Li L, Xu BQ (2004) Electrochim Acta 50:1
19. Rolison DR, Hagans PL, Swider KE, Long JW (1999) Langmuir 15:774
20. Chen ZG, Qiu XP, Lu B, Zhang SC, Zhu WT, Chen LQ (2005) Electrochem Commun 7:593
21. Jeon MK, Won JY, Woo SI (2007) Electrochem Solid State Lett 10:B23
22. Papageorgopoulos DC, de Heer MP, Keijzer M, Pieterse JAZ, de Bruijn FA (2004) J Electrochem Soc 151:A763
23. Rolison DR (2003) Science 299:1698
24. Stroud RA, Long JW, Swider-Lyons KE, Rolison DR (2002) Microsc Microanal 8:50
25. Ren XM, Wilson MS, Gottesfeld S (1996) J Electrochem Soc 143:L12
26. Lu Q, Yang B, Zhuang L, Lu J (2005) J Phys Chem B 109:8873

27. Lu Q, Yang B, Zhuang L, Lu J (2005) J Phys Chem B 109:1715
28. Wilson MS, Garzon FH, Sickafus KE, Gottesfeld S (1993) J Electrochem Soc 140:2872
29. Mukerjee S, Srinivasan S (1993) J Electroanal Chem 357:201
30. Antolini E (2003) J Mater Sci 38:2995
31. Antolini E, Salgado JRC, Gonzalez ER (2006) J Power Sources 160:957
32. Borup R, Meyers J, Pivovar B, Kim YS, Mukundan R, Garland N, Myers D, Wilson M, Garzon F, Wood D, Zelenay P, More K, Stroh K, Zawodzinski T, Boncella J, McGrath JE, Inaba M, Miyatake K, Hori M, Ota K, Ogumi Z, Miyata S, Nishikata A, Siroma Z, Uchimoto Y, Yasuda K, Kimijima K, Iwashita N (2007) Chem Rev 107:3904
33. Bezzerra WB, Zhang L, Liu H, Lee K, Marques ALB, Marques EP, Wang H, Zhang J (2007) J Power Sources 173:891
34. Piela P, Eickes C, Brosha E, Garzon F, Zelenay P (2004) J Electrochem Soc 151:A2053
35. Gancs L, Hult BN, Hakim N, Sanjeev Mukerjee S (2007) Electrochem Solid State Lett 10:B150
36. Holstein WL, Rosenfeld HD (2005) J Phys Chem B 109:2176
37. Park G-S, Pak C, Chung Y-S, Kim J-R, Jeon WS, Lee Y-H, Kim K, Chang H, Seung D (2008) J Power Sources 176:484
38. Guo J, Sun G, Wu Z, Sun S, Yan S, Cao L, Yan Y, Su D, Xin Q (2007) J Power Sources 172:666
39. Chung Y, Pak C, Park G-S, Jeon WS, Kim J-R, Lee Y, Chang H, Seung D (2008) J Phys Chem C 112:313
40. Thomas SC, Ren X, Gottesfeld S, Zelenay P (2002) Electrochim Acta 47:3741
41. Chen W, Sun G, Liang Z, Mao Q, Li H, Wang G, Xin Q, Chang H, Pak C, Seung D (2006) J Power Sources 160:933
42. Chakraborty D, Chorkendorff I, Johannessen T (2007) J Power Sources 173:110
43. Shyam B, Arruda TM, Mukerjee S, Ramaker DE (2009) J Phys Chem C 113:19713
44. Park Y, Lee B, Kim C, Oh Y, Nam S, Park B (2009) J Mater Res 24:2762
45. Ma J, Yu J, Zhao D, Wang AJ, Xu BQ (2009) Chinese J Catal 30:485
46. Sun H-J, Ding L-X, Chen Y, Zhou Y-M, Lu T-H, Tang Y-W (2010) Chinese J Inorg Chem 26:25
47. Park J-Y, Scibioh MA, Kim S-K, Kim H-J, Oh I-H, Lee TG, Heung HY (2009) Int J Hydrogen Energy 34:2043
48. Wilson MS, Valerio JA, Gottesfeld S (1995) Electrochim Acta 40:355
49. Liu J, Zhou Z, Zhao X, Xin Q, Sun G, Yi B (2004) Phys Chem Chem Phys 6:134
50. Jeon MK, Lee KR, Oh KS, Hong DS, Won JY, Li S, Woo SI (2006) J Power Sources 158:1344
51. Jeon MK, Won JY, Oh KS, Lee KR, Woo SI (2007) Electrochim Acta 53:447
52. Lai C-M, Lin J-C, Hsueh K-L, Hwang C-P, Tsay K-C, Tsai L-D, Peng Y-M (2008) J Electrochem Soc 155:B843
53. Chen W, Sun G, Guo J, Zhao X, Yan S, Tian J, Tang S, Zhou Z, Xin Q (2006) Electrochim Acta 51:2391
54. Sarma LS, Chen C-H, Wang G-R, Hsueh K-L, Huang C-P, Sheu H-S, Liu D-G, Lee J-F, Hwang B-J (2007) J Power Sources 167:358
55. Wang Z-B, Rivera H, Wang X-P, Zhang H-X, Feng P-X, Lewis EA, Smotkin ES (2008) J Power Sources 177:386
56. Cha H-C, Chen C-Y, Shiu J-Y (2009) J Power Sources 192:451
57. Pourbaix M (1963) Atlas d'Equilibres Electrochimiques. Gauthier-Villars, Paris, p 346
58. Hadzi-Jordanov S, Angerstein-Kozlowska H, Vukoviff M, Conway BE (1978) J Electrochem Soc 125:1471
59. Gavrilov AN, Petrii OA, Mukovnin AA, Smirnova NV, Levchenko TV, Tsirlina GA (2007) Electrochim Acta 52:2775
60. Zhdanov VP, Kasenno B (2006) Electrochem Commun 8:561
61. Ryden WD, Lawson AW (1968) Phys Lett 26A:209
62. Swider KE, Merzbacher CI, Hagans PL, Rolison DR (1997) Chem Mater 9:1248
63. Chang K-H, Hu C-C (2004) J Electrochem Soc 151:A958
64. Gancs L, Hakim N, Hult B, Mukerjee S (2006) ECS Trans 3:607
65. Hyun M-S, Kim S-K, Lee B, Peck D, Shul Y, Jung D (2008) Catal Today 132:138
66. Yamada H, Shimoda D, Matsuzawa K, Tasaka A, Inaba M (2007) Meet Abstr - Electrochem Soc 702:454
67. Yamada H, Shimoda D, Tasaka A, Inaba M (2008) Meet Abstr-Electrochem Soc 802:826
68. Choban ER, Spendelow JS, Gancs L, Wieckowski A, Kenis PJA (2005) Electrochim Acta 50:5390
69. Ranga JS, Gancs L, Choban ER, Primak A, Natarajan D, Markoski LJ, Kenis PJA (2005) J Am Chem Soc 127:16758
70. Sugimoto W, Saida T, Takasu Y (2006) Electrochem Comm 8:411
71. Saída T, Sugimoto W, Takasu Y (2010) Electrochim Acta 55:857
72. Zheng JP, Cyang PJ, Jow TR (1995) J Electrochem Soc 142:2699
73. Cabello-Moreno N, Crabb EM, Fisher JM, Russell AE, Thompsett D (2009) Meet Abstr-Electrochem Soc 902:983
74. Wang S, Wang X, Jiang SP (2008) Langmuir 24:10505
75. Liu S-H, Yu W-Y, Chen C-H, Lo A-Y, Hwang B-J, Chien S-H, Liu S-B (2008) Chem Mater 20:1622
76. Shimazaki Y, Kobayashi Y, Sugimasa M, Yamada S, Itabashi T, Miwa T, Konno M (2006) J Colloid Interface Sci 300:253
77. Tian J, Sun G, Jiang L, Yan S, Mao Q, Xin Q (2007) Electrochem Comm 9:563
78. Ma J-H, Feng Y-Y, Zhang G-R, Wang A-J, Xu B-Q (2010) Electrochem Comm (in press)
79. Park Y, Lee B, Kim C, Kim J, Park B (2009) J Mater Res 24:140
80. Zhang J, Sasaki K, Sutter E, Adzic RR (2007) Science 315:220
81. Liang ZX, Zhao TS, Xu JB (2008) J Power Sources 185:166